DS-OCDMA Encoder/Decoder Performance Analysis Using Optical Low-Coherence Reflectometry

Ihsan Fsaifes, Catherine Lepers, Anne-Francoise Obaton, and Philippe Gallion, *Senior Member, IEEE*

***Abstract*—Direct-sequence optical code-division multiple-access (DS-OCDMA) encoder/decoder based on sampled fiber Bragg gratings (S-FBGs) is characterized using phase-sensitive optical low-coherence reflectometry (OLCR). The OLCR technique allows localized measurements of FBG wavelength and physical length inside one S-FBG. This paper shows how the discrepancies between specifications and measurements of the different FBGs have some impact on spectral and temporal pulse responses of the OCDMA encoder/decoder. The FBG physical lengths lower than the specified ones are shown to affect the mean optical power reflected by the OCDMA encoder/decoder. The FBG wavelengths that are detuned from each other induce some modulations of S-FBG reflectivity resulting in encoder/decoder sensitivity to laser wavelength drift of the OCDMA system. Finally, highlighted by this OLCR study, some solutions to overcome limitations in performance with the S-FBG technology are suggested.**

***Index Terms*—Fiber Bragg grating (FBG), optical code-division multiple access (OCDMA), optical low-coherence reflectometry (OLCR).**

I. Introduction

MULTIPLE-ACCESS techniques are proposed to meet the growing demand for high-speed optical broadband access. Recently, much attention has been paid to optical code-division multiple-access (OCDMA) systems. They offer an all-optical processing, potential information security, and asynchronous access ability [1]. OCDMA techniques allow numerous signals from different users to occupy the same single-mode optical fiber transmission channel, optimizing the use of the wide available bandwidth. The key components of OCDMA systems consist of the encoder and the decoder that perform all-optical code generation and data recognition, respectively. A code or sequence of pulses referred to as "chips" is attributed to each user to encode its data bits. The encoded data are then broadcasted into the network and are only recognized by the matched decoder.

Depending on the coding approach, various OCDMA technique implementations have been proposed. These are temporal encoding, which is also known as direct-sequence encoding (DS-CDMA) [2], spectral phase and/or amplitude encoding [3], [4], two-dimensional (2-D) encoding [5], and hybrid encoding [6]. Most encoders/decoders of the OCDMA systems are implemented with fiber Bragg gratings (FBGs) because of their ready integrability, compactness, and low fabrication cost. In the direct detection DS-OCDMA system considered here, the encoder/decoder is achieved with sampled FBGs (S-FBGs) [7]. An S-FBG is a grating with a periodic superstructure in which the period is varied periodically with a period that is much larger than the nominal grating period Λ. Such "sampled" gratings have been proposed and demonstrated for numerous applications, including dense wavelength-division multiplexing (DWDM) [8]–[10].

To evaluate the performances of OCDMA systems, bit-error-rate (BER) transmission measurements are currently performed. Channel physical parameters such as chromatic dispersion, noise, and multiple-access interference (MAI) have been shown to strongly influence the quality of the transmission [11], [12]. However, until now, very few interests had been paid on the impact of encoder/decoder technological features on the transmission performances. Recently, effects of encoder/decoder mismatch due to wavelength and chip time misalignments on performances of a fast frequency hopping OCDMA system have been numerically investigated [13]. In this 2-D wavelength–time $(\lambda - t)$ technique, the code is defined by multiple wavelengths, where each of them is delayed by a multiple of time chip. The observed misalignments are shown to be responsible for a reduced optical power level to be received, affecting the signal-to-noise ratio (SNR) and, consequently, the BER performances of the OCDMA system. In the work reported here, we focus our attention on the experimental determination of the technological parameters of the DS-OCDMA encoder/decoder, and we study their direct impact on spectral and temporal code responses. The parameters are measured using the optical low-coherence reflectometry (OLCR) technique, which appears to be a powerful tool to analyze the discrepancies between the specified and realized encoder/decoder. The impact of these differences on the performance of the OCDMA encoder/decoder is studied and is taken into account to suggest improved design and implementation of the OCDMA encoder/decoder.

The OLCR technique is a highly efficient nondestructive characterization method for optical components such as laser diodes, modulators, FBGs, and, more recently, photonic crystal

Manuscript received February 21, 2006; revised May 9, 2006.

I. Fsaifes and P. Gallion are with the Ecole Nationale Supérieure des Télécommunications (GET/Télécom Paris), 75013 Paris, France (e-mail: fsaifes@enst.fr; gallion@enst.fr).

C. Lepers is with the Laboratoire de Physique des Lasers, Atomes et Molécules, Universite de Lille, 59655 Villeneuve d' Ascq Cedex, France (e-mail: Catherine.Lepers@univ-lille1.fr).

A.-F. Obaton is with the Laboratoire National de Métrologie et d'Essais, 78197 Trappes Cedex, France (e-mail: anne-francoise.obaton@lne.fr).

Digital Object Identifier 10.1109/JLT.2006.878039

fibers [14]–[19]. The OLCR technique is basically a Michelson interferometer illuminated with a broadband light source. A translating mirror ends one of its arms, and the device under test ends the other. The peaks in the recorded reflectograms are related to localized reflections whose position is determined by equal optical path differences (OPDs) between the two arms.

In this paper, the measured reflectograms allow to achieve precise and localized measurements of the different FBG parameters inside one encoder/decoder. The complex reflection spectra of the devices calculated from the interferogram data give physical length and wavelength information of the different FBGs of the encoder/decoder.

We point out Bragg wavelength mismatches between FBGs. This feature is shown to induce modulation of the reflectivity in the encoder/decoder spectral response. This leads to optical powers per pulse dependent on the wavelength drift of the laser source used in the DS-OCDMA system.

We show that FBG physical lengths are significantly different from specified ones, and we explain this feature. A detailed analysis of the index modulation amplitude depths considered during the realization of the devices reveals some discrepancies, too. These two impairments lead to a lower reflectivity for each FBG affecting the total mean reflected optical power of the encoder/decoder.

This paper is organized as follows: In the second section, we present specifications and realization of the studied DS-OCDMA encoder/decoder. In the third section, we describe the phase-sensitive OLCR experimental setup used to characterize the encoder/decoder, and we give the obtained measurements after analyzing reflectograms and spectral responses of the different FBGs. In the fourth section, the impact of the measured parameters detuned from specified ones on encoder/decoder spectral and temporal responses is studied. Finally, we provide some useful discussions and conclusions.

II. DS-OCDMA Encoder/Decoder Fabrication

To generate an ON–OFF-keying codeword C (100010001), an S-FBG (FBG_1, FBG_2, FBG_3) that reflects a user-data 50-ps pulse train (Fig. 1) has been designed and realized by exposure of the fiber to ultraviolet (UV) laser light with the phase mask method [20]. Each "1" chip of the codeword results from the reflection of an incident pulse by a 500-μm-long FBG. A typical 21 500-μm optical fiber length between two successive FBGs is proportional to chip time duration. The period of the superstructure corresponds to four chip time durations. The first FBG_1 reflectivity coefficient R_1 must be sufficiently weak in order to transmit the pulses through the total length of the S-FBG. C code is generated from the S-FBG at the 1551-nm Bragg wavelength. This code design must permit to obtain ideal code sequences with equal optical power pulses reflected from the encoder/decoder.

The encoder/decoder technological realization is achieved by UV photoinscription of FBGs with the phase mask technique, which is the widely robust and stable method used for reproducible FBG fabrication. As all the FBGs of one encoder/decoder are tuned to the same wavelength, this method is particularly well adapted as it is not needed to change

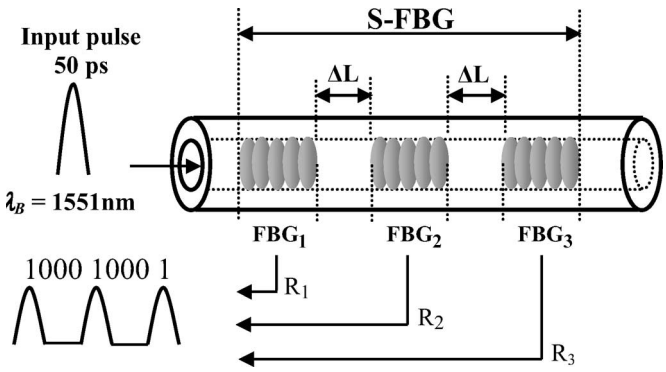

Fig. 1. S-FBG encoder/decoder design.

the mask. The UV source is a KrF pulsed laser working at $\lambda_{\mathrm{UV}} = 248$ nm with frequency rate $F_r = 20$ Hz. To increase their photosensitivity before UV irradiation, optical fibers have been hydrogen-loaded at a maximal pressure of 140 atm and a temperature of 110 °C carried out for 3 days. Depending on the fiber used and on the hydrogenation process, the average fluence per pulse after the phase mask is around 160 ± 20 mJ/cm^2. The FBGs have been written within the H_2-loaded fiber through a phase mask with a pitch of $\Lambda = 1071.6$ nm to obtain a Bragg wavelength resonance at 1551 nm.

The grating with the highest reflectivity FBG_3 ($R_3 = 34\%$ and $\Delta n_3 = 10^{-3}$) has been firstly written with a typical physical length of 500 μm. During the inscription, the growth kinetics curve of the evolution of the refractive-index modulation amplitude Δn_{mod} (i.e., the grating reflectivity R_i) as a function of the number of the UV writing pulses of light N_i has been recorded. The fiber has then been moved along its axis over a length corresponding to the required "0" chip sequence, and FBG_2 ($R_2 = 24\%$ and $\Delta n_2 = 8 \times 10^{-4}$) has been written. The third grating FBG_1 ($R_1 = 16\%$ and $\Delta n_1 = 6.4 \times 10^{-4}$) has then been written following a similar process. To accurately control the fiber length separating two consecutive gratings, the fiber was mounted on a piezo translation stage with an interferometric rule. The accuracy of the FBG positioning is in the micrometer range.

III. OLCR Characterization

To fulfil the analysis of the discrepancies between specified and experimental parameters, we use the OLCR technique to obtain precise measurements of the following encoder/decoder parameters: FBG Bragg wavelengths λ_B and physical lengths L_{FBG}. The evolution of FBG reflectivity rates is achieved from the analysis of the growth kinetics curve.

A. Experimental Setup

The OLCR setup shown in Fig. 2 is basically a Michelson interferometer with a movable reference mirror in one arm and the device under test in the second. It includes a two-by-two coupler: The source and the detector are located on one side, and the test and reference arms on the other side. The reference arm includes a movable corner cube mounted on an airborne-translation stage so that the OPD of the interferometer

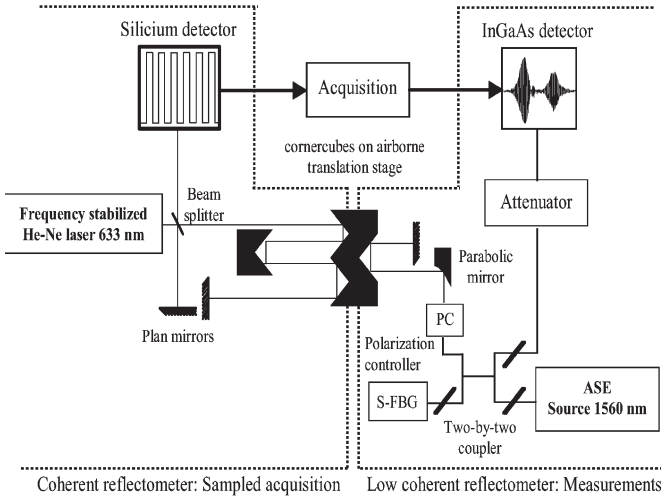

Fig. 2. Phase-sensitive OLCR setup.

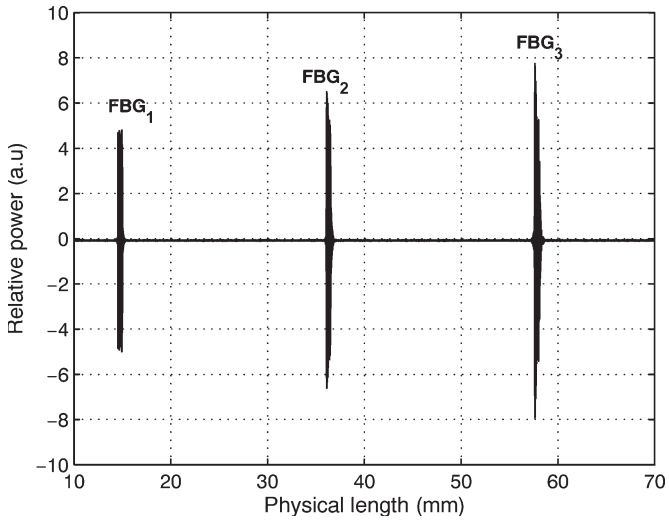

Fig. 3. Different FBG reflectograms inside the S-FBG encoder.

can be tuned. An amplified spontaneous emission (ASE) source based on an Er^{3+}-doped fiber amplifier with a flat-top spectrum allows characterization of the S-FBG over the entire $C+L$-band (i.e., 1525–1605 nm spectral range). The reflectogram is obtained by varying the OPD between the two arms of the interferometer at a constant velocity. When the OPD between a reflection point inside the encoder/decoder and the moving mirror is lower than the coherence length of the source, an interference signal is produced. Due to the low-coherence property of the source, the interference pattern spreading, which is reciprocal to the source spectral linewidth, is small enough to accurately probe the fiber at the null OPD location. In order to recover information on the phase, the reflectogram needs to be sampled with equally spaced and well-calibrated steps.

A coherent free interferometer incorporating a frequency-stabilized He–Ne laser fulfils this requirement. The two interferometers have a common part that holds the moving mirrors mounted on the airborne-translation stage. The sine-wave signal generated by the coherent interferometer is square-reshaped. A data point from the low coherent reflectometer is then acquired on each ascending front of the ADC-converted signal, which corresponds to a sampling step of 80 nm. The S-FBG under test is placed in the measurement arm of the OLCR, and the movable mirror is displaced. The obtained reflectogram is essentially a Fourier transform of FBG complex reflectivity.

B. OLCR Measurements

To characterize the DS-OCDMA encoder/decoder, the entire S-FBG has been scanned ten successive times in order to estimate standard deviation between measurements. Three interferograms were obtained corresponding to the three FBGs that compose the encoder/decoder (Fig. 3). FBGs present different reflectivity rates in an increasing order. This optimization permits to achieve pulses code with equal reflected power amplitude.

In Fig. 4, we give FBG relative reflectivities of the S-FBG encoder and the corresponding S-FBG decoder measured with the OLCR technique. These spectra are calculated from

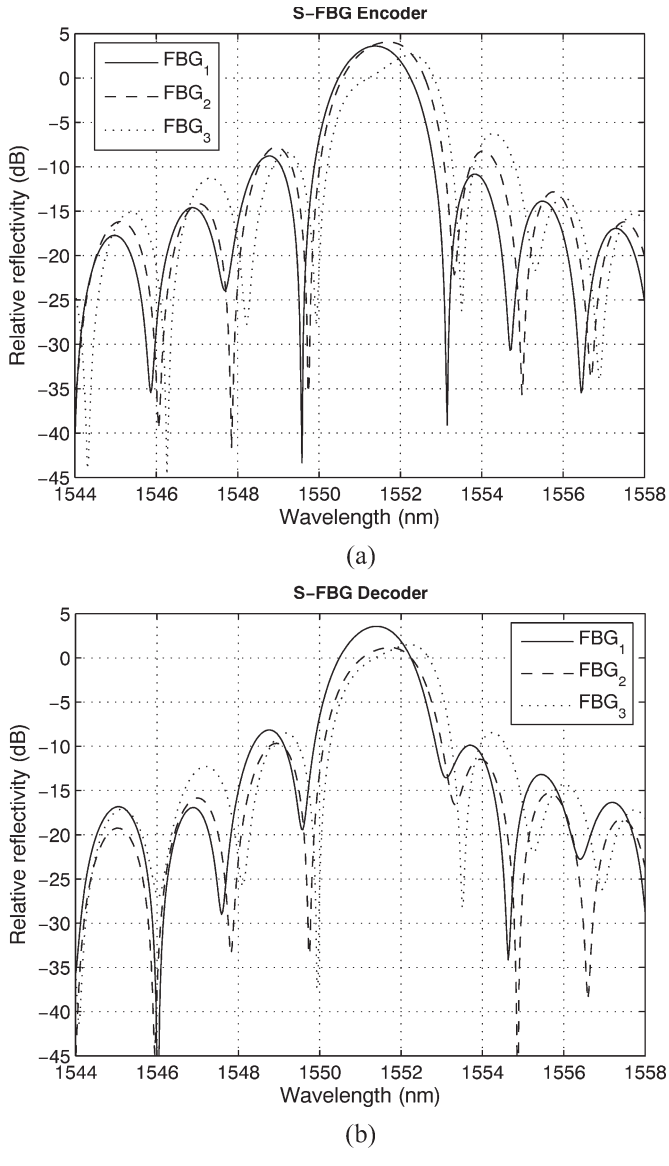

Fig. 4. FBG relative reflectivities of S-FBG encoder/decoder versus wavelength.

TABLE I
OLCR MEASUREMENTS FOR THE S-FBG ENCODER

	S-FBG encoder
FBG_1	L_{FBG1}= 459 ± 2 μm λ_{B1} = 1551.38 ± 0.13 nm
FBG_2	L_{FBG2}= 456 ± 2 μm λ_{B2} = 1551.53 ± 0.13 nm
FBG_3	L_{FBG3} = 459 ± 2 μm λ_{B3} = 1551.69 ± 0.07 nm

interferogram data using a fast Fourier transform algorithm and give Bragg wavelength information of the different FBGs inside the encoder/decoder.

It clearly appears from these measurements that FBG Bragg wavelengths are detuned differently from each other. For the S-FBG encoder, FBGs are centered at 1551.38, 1551.53, and 1551.69 nm, respectively. Whereas for the S-FBG decoder, FBGs are centered at 1551.34, 1551.54, and 1551.71 nm, respectively. Consequently, the encoder and the decoder will not be exactly matched, each having a different mean Bragg wavelength.

The FBG bandwidth is defined as the spectral width of the Bragg main peak. The full bandwidth $\Delta\lambda_{\mathrm{FBG}}$ measured between the zeros on either side of the main peak is given by [21]

$$\Delta\lambda_{\mathrm{FBG}} = \frac{\lambda_B^2}{\pi n_{\mathrm{eff}} L_{\mathrm{FBG}}} \left[\left(\kappa L_{\mathrm{FBG}}\right)^2 + \pi^2 \right]^{1/2}$$

where κ is the coupling coefficient defined as

$$\kappa = \frac{\pi \Delta n_{\mathrm{mod}}}{\lambda_B} \eta(V)$$

where $\eta(V)$, as a function of the fiber-normalized frequency V, is the modal overlap factor of the LP_{01} mode in the fiber core. For standard telecommunication single-mode fibers, $1.5 \leq V \leq 2.4$, which corresponds to $0.55 \leq \eta \leq 0.82$.

As the FBGs considered here present weak reflectivities, we have verified that $((\kappa L_{\mathrm{FBG}})^2 \ll \pi^2)$ ($(\kappa L_{\mathrm{FBG}})^2$ is equal to 0.18, 0.28, and 0.45 for FBG_1, FBG_2, and FBG_3, respectively). In that case, the expression of the full bandwidth $\Delta\lambda_{\mathrm{FBG}}$ may be simplified and becomes an inverse function of the FBG physical length L_{FBG}. From $\Delta\lambda_{\mathrm{FBG}}$ measurements, we have calculated FBG physical lengths as

$$L_{\mathrm{FBG}} = \frac{\lambda_B^2}{n_{\mathrm{eff}} \Delta\lambda_{\mathrm{FBG}}}$$

where $n_{\mathrm{eff}} = 1.447$ is the value of the effective modal index of the LP_{01} mode at 1551 nm.

However, let us note that for exact FBG physical length estimation, the material and the waveguide dispersion have to be taken into account. Thus, physical lengths are evaluated using the group index of refraction $n_g = 1.468$ instead of the effective index $n_{\mathrm{eff}} = 1.447$.

In Table I, we give the parameter values measured with the OLCR technique for the S-FBG encoder. Measured Bragg wavelengths and FBG physical lengths are given with a standard deviation obtained from ten successive measurements.

We may notice that FBG physical lengths are detuned from the specified value of 500 μm. This is due to the photoinscription technique. A phase mask is a diffractive optical element that spatially modulates the UV writing beam. The profile of the periodic grating corrugation is chosen to suppress the zeroth-order diffracted beam to less than 5% of the transmitted beam. On the contrary, the diffracted plus and minus first orders are maximized (35% of the transmitted optical power). A near-fringe pattern is produced by the interference of the plus and minus first-order diffracted beams. This pattern photoinduces a refractive-index modulation in the core of a photosensitive optical fiber placed in close proximity, i.e., immediately behind the phase mask. In that configuration, the period of the mask is related to the writing wavelength by [22]

$$\Lambda = \frac{\lambda_{\mathrm{UV}}}{2\,\sin(\theta/2)}.$$

If the FBGs were exactly placed on the phase mask, their physical length should be 500 μm, which is not the case as we want to translate them spatially in order to write successive FBGs. The near-field interference fringe pattern describes a triangular shape whose basis is delimited by the slit width equal to 500 μm. In close proximity, this distance decreases and can be equal to 459 or 456 μm. A simple calculation permits to evaluate that the fiber was from 175.9 μm for FBG_1 and FBG_3 and 188.8 μm for FBG_2 from the phase mask plane. The fact that FBG_2's physical length is less than FBG_1's and FBG_3's lengths can be explained as follows: As the fiber is maintained in two points on an interferometric rule, which will be translated to write successive FBGs, a slight curvature may occur in the middle of the fiber, and FBG_2 is then moved farther from the phase mask plane.

Consequently, fiber lengths between FBGs have been measured to be larger than the specified values. Fiber lengths are strongly related to phase variations of the electric field of multiple reflected pulses from the device, which sometimes superimpose within a pulse time duration. Such impairments due to the multipath interferometer behavior of the encoder/decoder related to the coherence of the DS-OCDMA system have been studied in [23].

To explain the origin of Bragg wavelength mismatches between FBGs inside the encoder/decoder, we have analyzed the evolution of the Bragg wavelength λ_B of different FBGs as a function of the number of writing pulses N_i (Fig. 5). As each FBG is written with a different refractive-index modulation amplitude Δn_{mod} (i.e., a different number N_i of writing pulses), the Bragg wavelengths of the FBGs are detuned from each other. The Bragg wavelength detunings between the three gratings $(\mathrm{FBG}_{1,2,3})$ are given as follows: $\delta\lambda_{1,2} = 0.22$ nm, $\delta\lambda_{2,3} = 0.21$ nm, and $\delta\lambda_{1,3} = 0.43$ nm.

Before the UV photoinscription process, the fiber is hydrogen-loaded by diffusing hydrogen molecules at high pressure. The reaction of hydrogen molecules at the germanium sites produces germanium oxygen deficiency when exposed to UV light. Hydrogen concentration resulting from diffusion

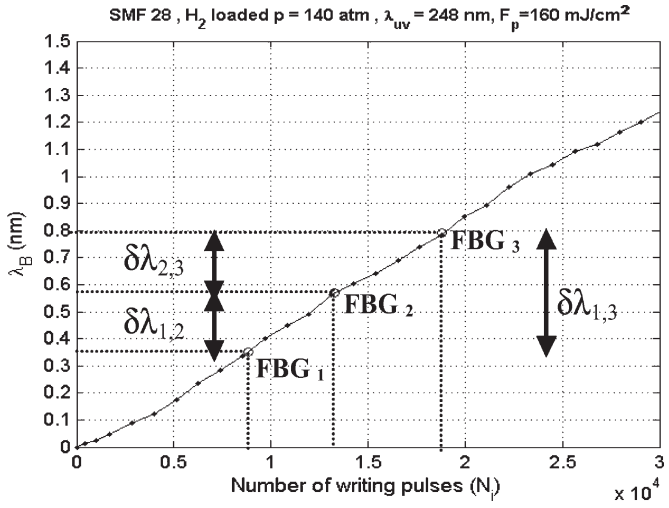

Fig. 5. Evolution of the different FBG wavelengths of an S-FBG encoder as a function of the number of the writing pulses N_i.

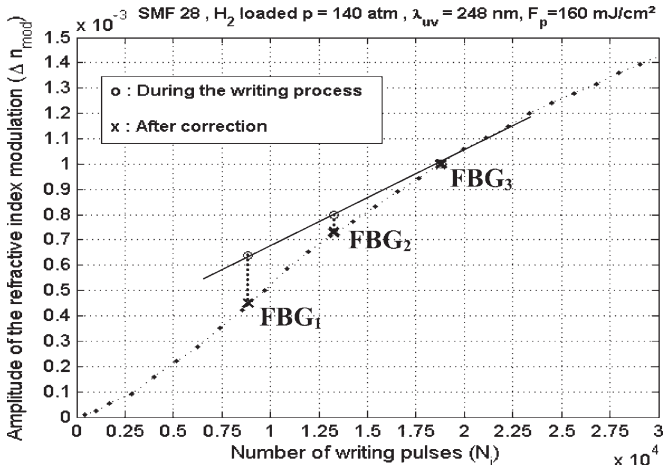

Fig. 6. Evolution of the different FBG specified index modulation depths ($\circ$) and the corrected index modulation depths (x) inside an S-FBG encoder as a function of the number of writing pulses N_i.

and reaction with defects in the glass induces a shift in the FBG Bragg wavelength. This shift is estimated to be 1.5 nm. This value must be added to the initial Bragg wavelength ($\lambda_{Bi} = 1549.5$ nm) of an FBG written in a nonhydrogen fiber. The final Bragg wavelength after hydrogenation is 1551 nm. Furthermore, as FBGs are written with different UV light pulse numbers N_i, additional Bragg wavelength shift is induced for each one. From Fig. 5, we can calculate that the Bragg wavelengths of each FBG are 1551.35, 1551.57, and 1551.79 nm, respectively. These measurements are in good agreement with those measured with the OLCR technique.

From the growth kinetics curve displayed in Fig. 6, FBG_3 is written with an index modulation depth $\Delta n_3 = 10^{-3}$ to achieve the specified 34% FBG_3 reflectivity. As coordinates Δn_2 and Δn_1 and their corresponding number of writing pulses N_2 and N_1 are deduced with a simple linear regression, we note that they do not match exactly with the growth kinetics curve, and thus, a first correction to the reflectivities of the different FBGs with the specified values is needed.

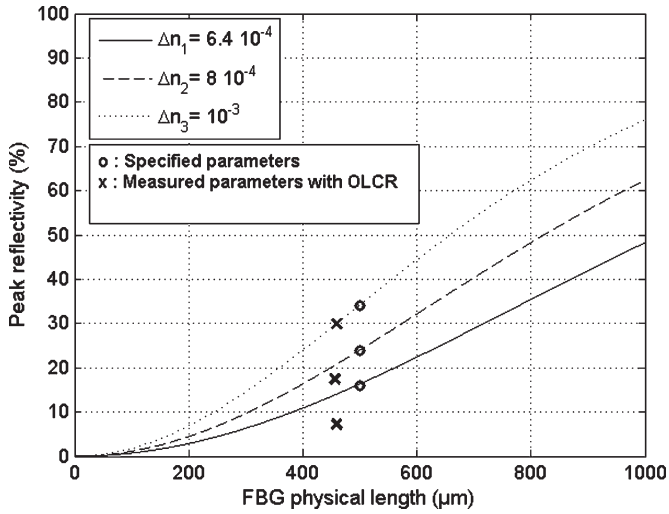

Fig. 7. FBG peak reflectivity versus FBG physical length L_{FBG} inside an S-FBG encoder.

With OLCR measurements, we are now able to calculate the peak reflectivity R_{peak} of each FBG at λ_B Bragg wavelength following the formula written as follows:

$$R_{\mathrm{peak}} = \tanh^2(\kappa L).$$

In Fig. 7, the evolution of peak reflectivity R_{peak} as a function of the FBG physical length L_{FBG} and index modulation amplitudes Δn_1, Δn_2, and Δn_3 for $\lambda_B = 1551$ nm and $\eta = 0.66$ are drawn. We first localize the different FBG reflectivities obtained by simulation ($\circ$ in Fig. 7). Taking into account the corrected index modulation depths extracted from the analysis of the growth kinetics curve, reflectivities less than 24% and 16% for FBG_2 and FBG_1, respectively, are calculated. Taking into account the different measured parameters with OLCR, we note that the reflectivity of each FBG is still reduced (x in Fig. 7). The mean reflected power of the encoder and the decoder is around 8%. It is the reason why we observe encoder temporal response with lower reflected mean optical power. This does drastically not change the behavior of the system [24]. Nevertheless, in future realization of devices, these observed impairments will be taken into account.

IV. Experimental Responses of the S-FBG Encoder/Decoder

Spectral response of the S-FBG encoder/decoder has been measured in reflection by using ASE from an erbium-doped fiber (Fig. 8). We can observe that the central Bragg wavelength of the encoder and the decoder are different: The S-FBG encoder is centered at 1551.33 nm and the S-FBG decoder at 1551.55 nm. Let us notice that the wavelength difference between the encoder and the decoder must be less than half the spectral width at half maximum of the S-FBG photonic band gap (~ 0.8 nm) to properly reconstruct the encoded pulse.

In Fig. 8, we also observe that the spectral responses of the encoder and the decoder present a rapidly varying envelope. The reflectivity is sine-wave-modulated at $\Delta\sigma$ wavelength

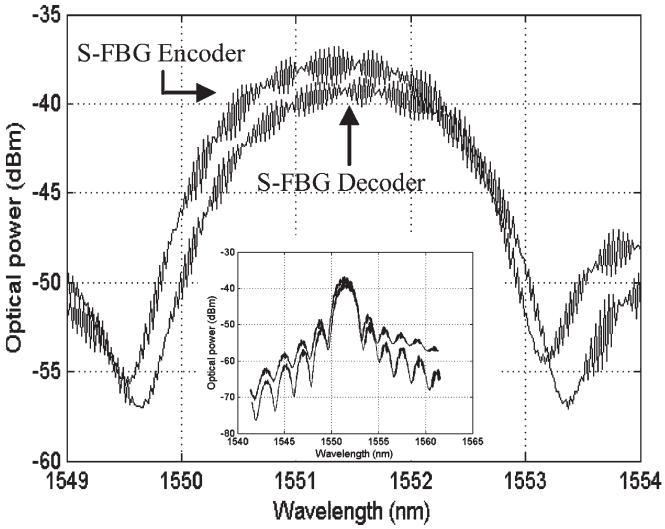

Fig. 8. Experimental spectral responses of the S-FBG encoder and decoder.

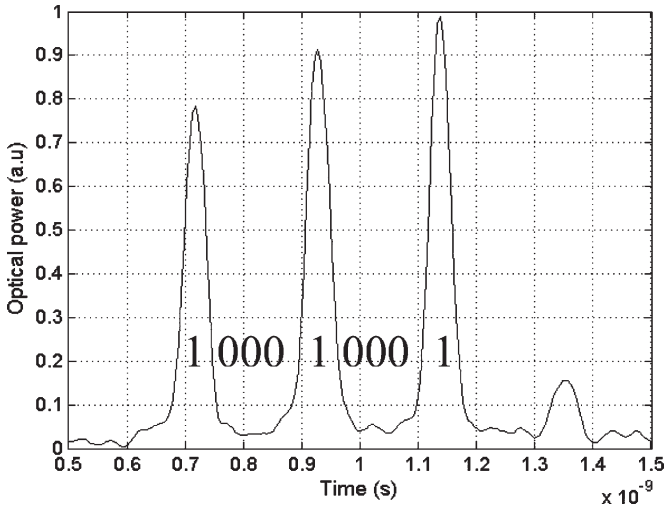

Fig. 9. Experimental temporal response of the S-FBG encoder.

directly related to the length of the Fabry–Pérot cavities ΔL determined by $\mathrm{FBG}_1 - \mathrm{FBG}_2$ and $\mathrm{FBG}_2 - \mathrm{FBG}_3$, i.e.,

$$\Delta\sigma \approx \frac{\lambda_B^2}{2n_{\mathrm{eff}}\Delta L} \approx 0.04 \text{ nm}.$$

A relative high sensitivity of the device reflectivity will be observed if the wavelength of the laser source drifts.

We have previously shown that Bragg wavelength mismatches between FBGs are due to the fabrication process as each FBG is written with a different index modulation depth. FBG wavelength is also sensitive to temperature. A temperature change involves a variation in the Λ grating period, which induces a shift in Bragg wavelength $\lambda_B = 2n_{\mathrm{eff}}\Lambda$ [25], [26]. To avoid additional wavelength thermal drift in the encoder/decoder, we protect them within an appropriate package. In those conditions, the temperature variations have no significant impact on the performances of the system.

The experimental temporal response of the S-FBG encoder displays three main pulses with different optical powers (Fig. 9). The "1" pulses of the code sequence have a 50-ps full-width at half-maximum (FWHM) and are separated by 150 ps corresponding to three chip time durations. The observed fourth small extra peak is due to secondary reflections between the two Fabry–Pérot cavities determined by $\mathrm{FBG}_1 - \mathrm{FBG}_2$ and $\mathrm{FBG}_2 - \mathrm{FBG}_3$ involved in the design of the encoder. The optical power of the third pulse of the code is not relevant as it is due to spurious interferometric effects.

We get some interest for the two first pulses of the code sequence whose optical power levels are only related to FBG parameter measurements performed with OLCR. They will vary with the laser source wavelength as the mismatches between FBG Bragg wavelengths induce a modulation of the S-FBG reflectivity. The mean optical power of these pulses depends directly of FBG physical length as demonstrated above.

The lowering of the mean optical power and the variations of the quasi-instantaneous optical power of the code sequence pulses of the encoder/decoder devices will affect the autocorrelation function of the DS-OCDMA system. In a system configuration with a pulsed laser source, the reconstructed pulses will present less mean optical power, which will degrade the optical budget and the BER performances of the DS-OCDMA system. Bragg wavelength mismatches between encoder and/or decoder will impact the quasi-instantaneous optical power of the main peak of the autocorrelation function such as its sidelobes.

V. Conclusion

In this paper, we have pointed out that an in-depth analysis of FBG properties of the DS-OCDMA encoder/decoder using the phase-sensitive OLCR technique allows a complete understanding of the observed spectral and temporal OCDMA code responses. By analyzing the interferograms of the S-FBGs, we have been able to measure precisely localized parameters of the DS-OCDMA encoder/decoder.

The recording of the growth kinetics curve of the index modulation amplitude versus the number of UV pulses and OLCR measurements of FBG physical lengths have permitted to evaluate FBG peak reflectivities. We have demonstrated that impairments between specified and experimental values have contributed to lower the mean optical power of the pulses of the temporal code sequences.

We have also shown that the Bragg wavelength mismatches between FBGs induce sine-wave modulation of the reflectivity of the encoder/decoder and, consequently, leads to different instantaneous optical power levels observed in the encoder/decoder temporal response as the laser source wavelength of the DS-OCDMA system fluctuates.

Finally, technological limitations and tradeoffs in performance with the S-FBG technology have been identified. Discrepancies of encoder/decoder temporal and spectral responses from ideal ones concern mean optical power lowering and quasi-instantaneous fluctuations of the pulses of the code sequence. However, mean optical power lowering is not critical because it can be corrected by considering accurate encoder/decoder simulations with well-adapted FBG physical length and by taking into account the growth kinetics curve during the fabrication of future devices. Power fluctuation is a more

important feature as it involves change in the design of the encoder/decoder. To overcome Bragg wavelength mismatch between the encoder and/or the decoder due to the different numbers of UV pulses used for FBG photoinscription, we will write FBGs with the same index modulation depth, and we vary FBG physical lengths by placing an adjustable slit in front of the phase mask. In this case, the FBGs will be longer, but progress made in the long FBG fabrication technique should make this experiment feasible.

REFERENCES

[1] J. A. Salehi, "Code division multiple access techniques in optical fiber networks.1. Fundamental principles," *IEEE Trans. Commun.*, vol. 37, no. 8, pp. 824–833, Aug. 1989.

[2] P. R. Prucnal, M. A. Santoro, and T. R. Fan, "Spread spectrum fiber-optic local area network using optical processing," *J. Lightw. Technol.*, vol. LT-4, no. 5, pp. 547–554, May 1986.

[3] V. J. Hernandez, Y. Du, W. Cong, R. P. Scott, K. Li, J. P. Heritage, Z. Ding, B. H. Kolner, and S. J. B. Yoo, "Spectral phase-encoded time-spreading (SPECTS) optical code-division multiple access for terabit optical access networks," *J. Lightw. Technol.*, vol. 22, no. 11, pp. 2671–2679, Nov. 2004.

[4] Z. Wei, H. M. H. Shalaby, and H. Ghafouri-Shiraz, "Modified quadratic congruence codes for fiber Bragg grating based spectral-amplitude-coding optical CDMA systems," *J. Lightw. Technol.*, vol. 19, no. 9, pp. 1274–1281, Sep. 2001.

[5] H. Fathallah, L. A. Rusch, and S. LaRochelle, "Passive optical fast frequency-hop CDMA communications system," *J. Lightw. Technol.*, vol. 17, no. 3, pp. 397–405, Mar. 1999.

[6] P. C. The, M. Ibsen, J. H. Lee, P. Petropoulos, and D. J. Richardson, "Demonstration of a four channel WDM/OCDMA system using 255-chip 320-Gchip/s quarternary phase coding gratings," *IEEE Photon. Technol. Lett.*, vol. 14, no. 2, pp. 227–229, Feb. 2002.

[7] I. Fsaifes, M. Lourdiane, C. Lepers, R. Gabet, V. Beugin, and P. Gallion, "Performances of 1 Gb/s optical DS-CDMA based on sampled fiber Bragg gratings," in *Proc. SPIE*, 2005, vol. 5970, pp. 713–718.

[8] K. O. Hill, B. Malo, F. Bilodeau, D. C. Johnson, and J. Albert, "Bragg gratings fabricated in monomode photosensitive optical fiber by UV exposure through a phase mask," *Appl. Phys. Lett.*, vol. 62, no. 10, pp. 1035–1037, Mar. 1993.

[9] J. Eggleton, P. A. Krug, L. Poladian, and F. Ouellette, "Long periodic superstructure Bragg gratings in optical fibers," *Electron. Lett.*, vol. 30, no. 19, pp. 1620–1622, Sep. 1994.

[10] J. Martin, M. Tetu, C. Latrasse, A. Bellemare, and M. A. Duguay, "Use of a sampled Bragg grating as in-fiber optical resonator for the realization of a referencing optical frequency scale for WDM communications," presented at the Optical Fiber Communications Conf., Dallas, TX, Feb. 16–21, 1997, Paper ThJ5.

[11] S. Shen, A. M. Weiner, G. D. Sucha, and M. L. Stock, "Bit error rate performance of ultrashort-pulse optical OCDMA detection under multi-access interferences," *Electron. Lett.*, vol. 36, no. 21, pp. 1795–1797, Oct. 2000.

[12] X. Wang and K. Kitayama, "Analysis of beat noise in coherent and incoherent time-spreading OCDMA," *J. Lightw. Technol.*, vol. 22, no. 10, pp. 2226–2235, Oct. 2004.

[13] R. Adams and L. R. Chen, "Effect of encoder-decoder mismatch due to wavelength and time misalignments on the performance of two-dimensional wavelength-time optical code division multiple access systems," *Appl. Opt.*, vol. 44, no. 20, pp. 4368–4374, Jul. 2005.

[14] E. I. Petermann, J. Skaar, B. E. Sahlgren, R. A. H. Stubbe, and A. T. Friberg, "Characterization of fiber Bragg gratings by use of optical coherence domain reflectometry," *J. Lightw. Technol.*, vol. 17, no. 11, pp. 2371–2378, Nov. 1999.

[15] S. Mechels, K. Takada, and K. Okamoto, "Optical low coherence reflectometer for measuring WDM components," *IEEE Photon. Technol. Lett.*, vol. 11, no. 7, pp. 857–859, Jul. 1999.

[16] C. Palavicini, Y. Jaouën, G. Debarge, E. Kerrinckx, Y. Quiquempois, M. Douay, C. Lepers, A.-F. Obaton, and G. Melin, "Characterization of photonic crystal fiber properties using phase sensitive OLCR," *Opt. Lett.*, vol. 30, no. 4, pp. 361–363, Feb. 2005.

[17] K. Takada, I. Yokohama, K. Chida, and J. Noda, "New measurement system for fault location in optical waveguide devices based on an interferometric technique," *Appl. Opt.*, vol. 26, no. 9, pp. 1603–1606, May 1987.

[18] R. C. Youngquist, S. Carr, and D. E. N. Davies, "Optical coherence-domain reflectometry: A new optical evaluation technique," *Opt. Lett.*, vol. 12, no. 3, pp. 158–160, Mar. 1987.

[19] S. D. Dyer, K. B. Rochford, and A. H. Rose, "Fast and accurate low-coherence interferometric measurements of fiber Bragg grating dispersion and reflectance," *Opt. Express*, vol. 5, no. 11, pp. 262–266, Nov. 1999.

[20] D. Z. Anderson, V. Mizuehi, T. Erdogan, and A. E. White, "Production of in-fiber gratings using a diffractive optical element," *Electron. Lett.*, vol. 29, no. 6, pp. 566–568, Mar. 1993.

[21] T. Erdogan, "Fiber grating spectra," *J. Lightw. Technol.*, vol. 15, no. 8, pp. 1277–1294, Aug. 1997.

[22] P. E. Dyer, R. J. Farley, and R. Giedl, "Analysis of grating formation with excimer laser irradiated phase masks," *Opt. Commun.*, vol. 115, no. 3/4, pp. 327–334, Mar. 1995.

[23] I. Fsaifes, C. Lepers, M. Lourdiane, R. Gabet, and P. Gallion, "Pulsed laser source coherence time impairments in a direct detection DS-OCDMA system," presented at the CLEO Conf., Long Beach, CA, 2006, Paper CWH 6.

[24] P. Petropoulos, M. Ibsen, A. Fu, H. Geiger, R. L. Laming, and D. J. Richardson, "Coherent control of short pulses using fibre Bragg gratings," in *Proc. IEE Colloq. Opt. Fibre Gratings (Ref. No.1999/023)*, Mar. 26, 1999, pp. 8/1–8/6.

[25] H. Fathallah and L. A. Rusch, "Robust optical FFH-CDMA communications: Coding in place of frequency and temperature controls," *J. Lightw. Technol.*, vol. 17, no. 8, pp. 1284–1293, Aug. 1999.

[26] A. D. Kersey, M. A. Davis, H. J. Patrick, M. LeBlanc, K. P. Koo, C. G. Askins, M. A. Putnam, and E. J. Friebele, "Fiber grating sensors," *J. Lightw. Technol.*, vol. 15, no. 8, pp. 1442–1463, Aug. 1997.

Ihsan Fsaifes received the B.S. degree in electrical engineering from the Université des Sciences et Techniques de Blida, Blida, Algeria, in 1999 and the M.S. degree in digital communication systems from the Ecole Nationale Supérieure des Télécommunications, Paris, France, in 2003. He is currently working toward the Ph.D. degree in electronic and communication at the Ecole Nationale Supérieure des Télécommunications.

His research interests include fiber-optic communication systems, optical code-division multiple access (OCDMA), and all-optical processing technique using fiber Bragg gratings for OCDMA.

Catherine Lepers received the Ph.D. degree in physics from the University of Lille, Villeneuve d' Ascq, France, in 1993 for her research work on nonlinear dynamics in single-mode and weakly single-mode CO_2 lasers.

She joined the Nonlinear Optic Group, Laboratoire de Physique des Lasers, Atomes et Molécules (PhLAM), University of Lille, as an Associate Professor and worked on nonlinear spatiotemporal dynamics of lasers and nonlinear temporal dynamics of coupled lasers with saturable absorber. In 2000, she joined the Photonique Group in the same laboratory to do some studies on fiber Bragg gratings and on the characterization of photonic-crystal fibers. From 2002 to 2005, she was with Laboratoire LTCI, Ecole Nationale Supérieure des Télécommunications, performing advanced optical digital communications on code-division multiple-access (CDMA) techniques. Her present research topics include theory, conception, modeling, and characterization of optical CDMA devices in PhLAM and their applications in optical access networks in LTCI.

Anne-Francoise Obaton received the Ph.D. degree in physics from Université La Rochelle-France in 1998 for her research work titled, "New $Yb^{3+} - Er^{3+}$ codoped phosphate glasses for eye-safe laser applications."

In 1999, she had a postdoctoral position in the Laboratory for Integrated Micro-Mechatronic Systems, Institute of Industrial Science, Tokyo University, Tokyo, Japan, and worked on atomic force microscopy. Since 2000, she has been with the Laboratoire Nationale de Métrologie et d'Essais, Paris, France. Her research interest involves optical low-coherence reflectometry in the fiber-optic domain.

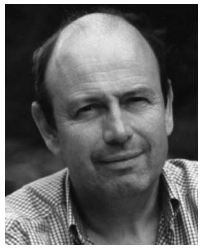

Philippe Gallion (M'82–SM'93) received the Doctorat de Troisième Cycle degree from the University of Reims, Reims, France, in 1975 and the Doctorat d'Etat degree from the University of Montpellier, Montpellier, France, in 1986.

He joined the Ecole Nationale Supérieure des Télécommunications (Télécom Paris), Paris, France, in 1978, where he is presently a Full Professor. He has made pioneering contributions on laser noise, injection locking, semiconductor laser modulation chirp and tuning, coherent systems and optical devices, and digital optical communications systems and networks. His present research topics include theory, conception, modeling, and characterization of functional devices and their applications in advanced optical digital communication systems and networks. He is author or coauthor of more than 150 technical papers and communications, and he has acted as Supervisor for more than 40 Ph.D. degree thesis.

Dr. Gallion is a member of the Optical Society of America. He is the Chairman of the IEEE Laser and Electro Optics Society (LEOS) French Chapter. He serves on the Editorial Board and Scientific Committee of several technical publications and as a member of Program or Steering Committee of international scientific meetings.